Analysis of hydraulic tomography using temporal moments of drawdown recovery data

Junfeng Zhu and Tian-Chyi J. Yeh

Department of Hydrology and Water Resources, University of Arizona, Tucson, Arizona, USA

Received 2 June 2005; revised 30 September 2005; accepted 21 October 2005; published 1 February 2006.

[1] Transient hydraulic tomography (THT) is a potentially cost-effective and high-resolution technique for mapping spatial distributions of the hydraulic conductivity and specific storage in aquifers. Interpretation of abundant well hydrographs of a THT survey, however, is a computational challenge. We take on this challenge by developing an estimation approach that utilizes the zeroth and first temporal moments of well hydrographs, instead of drawdown itself. The governing equations for the temporal moments are Poisson's equations. These equations demand less computational resources as opposed to the parabolic equation that governs drawdown evolution. Likewise, the adjoint equations for evaluating sensitivities of the moments for parameter estimation also take the same forms. Therefore a temporal moment approach is expected to expedite the interpretation of THT surveys. On the basis of this premise we extend our sequential successive linear estimator to use the zeroth moment and characteristic time of the drawdown-recovery data generated by THT surveys. We subsequently investigate computational efficiency and accuracy of the moment approach. Results of the investigation show that the temporal moment approach yields results similar to those from the approach that uses transient heads but at significantly less computational costs. Limitations using temporal moments are discussed subsequently.

Citation: Zhu, J., and T.-C. J. Yeh (2006), Analysis of hydraulic tomography using temporal moments of drawdown recovery data, *Water Resour. Res.*, *42*, W02403, doi:10.1029/2005WR004309.

1. Introduction

[2] Multiscale heterogeneity of geologic media is a rule rather than the exception. The knowledge of detailed spatial distributions of hydraulic properties is imperative to predict water and solute movement in the subsurface at high resolution [e.g., *Yeh*, 1992, 1998]. Traditional aquifer tests (e.g., pumping and slug tests) have been widely employed for estimating hydraulic properties of the subsurface for the last few decades. Besides their costly installation and invasive natures, *Beckie and Harvey* [2002] reported that slug tests can yield dubious estimates of the storage coefficient of aquifers. Validity of classical analysis for aquifer tests was also questioned by *Wu et al.* [2005]. They reported that the storage coefficient, S, value obtained from the traditional Theis analysis primarily represents a weighted average of S values over the region between the pumping and observation wells. In contrast to the S estimate, the transmissivity, T, estimate is a weighted average of all T values in the entire domain with relatively high weights near the pumping well and the observation well. In concordance with the finding by *Oliver* [1993], *Wu et al.* [2005] concluded that the T estimate can be influenced by any large-sized or strong anomaly within the cone of depression. Thus interpretation of the meaning of T estimates can be highly uncertain. As a result, previous assessments of transmissivity distributions of aquifers may be subject to serious doubt.

Copyright 2006 by the American Geophysical Union.
0043-1397/06/2005WR004309$09.00

[3] Hydraulic tomography [*Gottlieb and Dietrich*, 1995; *Yeh and Liu*, 2000; *Liu et al.*, 2002; *Bohling et al.*, 2002; *Zhu and Yeh*, 2005], based on the computerized axial tomography (CAT) scan concept of medical sciences, is potentially a viable technology for characterizing detailed spatial distributions of the hydraulic properties. Hydraulic tomography, in a simple term, is a series of cross-well interference tests. More precisely, hydraulic tomography involves stressing an aquifer by pumping water from or injecting water into a well, and monitoring the aquifer's response at other wells. A set of stress and response data yields an independent set of equations. Sequentially switching the pumping or injection location, without installing additional wells, results in a large number of aquifer responses induced by the stresses at different locations and thus a large number of independent sets of equations. This large number of sets of equations makes the inverse problem (i.e., using aquifer stress and response relation to estimate the spatial distribution of hydraulic parameters) better posed, and the subsequent estimates approach reality.

[4] Interpretation of hydraulic tomography surveys however is a numerical challenge. The large number of well hydrographs generated during tomography often leads to information overload, substantial computational burdens, and numerical instabilities [*Hughson and Yeh*, 2000]. To overcome these difficulties, *Yeh and Liu* [2000] developed a sequential successive linear estimator (SSLE) approach. This approach eases the computational burdens by sequentially including information obtained from different pumping tests; it resolves the nonuniqueness issue by providing

an unbiased mean of an abstracted stochastic parameter rather than the actual parameter. That is, it conceptualizes hydraulic parameter fields as spatial stochastic processes and seeks their conditional effective parameter distributions. The conditional effective parameters are conditioned on the data obtained from and governing physical principles of hydraulic tomography, as well as our prior knowledge of the geologic structure, and directly measured parameter values (such as from slug tests, or core samples). The SSLE approach in essence is the Bayesian formalism. Sand box experiments by *Liu et al.* [2002] and W. A. Illman et al. (Steady-state hydraulic tomography in a laboratory aquifer with deterministic heterogeneity: Multiscale validation of hydraulic conductivity tomograms, submitted to *Water Resources Research*, 2005) proved that the combination of hydraulic tomography and SSLE is a viable, cost-effective technique for delineating heterogeneity using a limited number of invasive observations. The work by *Yeh and Liu* [2000], nonetheless, is limited to steady state flow conditions, which may occur only under special field conditions. Because of this restriction their method ignores transient head data before flow reaches steady state conditions.

[5] Several researchers have investigated THT. *Bohling et al.* [2002] exploited the steady shape flow regime of transient flow data to interpret tomographic surveys. Similar to *Vasco et al.* [2000], *Brauchler et al.* [2003] developed a method that uses the travel time of a pneumatic pressure pulse to estimate air diffusivity of fractured rocks. As in X-ray tomography, their approach relies on the assumption that the pressure pulse travels along a straight line or a curved path. Thus an analytical solution can be derived for the propagation of the pressure pulse between a source and a pressure sensor. Many pairs of sources and sensors yield a system of one-dimensional analytical equations. A least squares based inverse procedure developed for seismic tomography can then be applied to the system of equations to estimate the diffusivity distribution. The ray approach avoids complications involved in numerical formulation of the three-dimensional forward and inverse problems, but it ignores interaction between adjacent ray paths and possible boundary effects. Consequently, their method requires an extensive number of iterations and pairs of source/sensor data to achieve a comparable resolution to that achieved from inverting a three-dimensional model. *Vesselinov et al.* [2001] applied an optimization technique and geostatistics to interpret pneumatic cross-borehole tests in fractured rocks.

[6] Recently, *Zhu and Yeh* [2005] extended the SSLE approach to THT to estimate both spatially varying hydraulic conductivity and specific storage fields in 3-D random media. They demonstrated that it is possible to obtain detailed hydraulic conductivity and specific storage fields of aquifers using few wells with THT surveys. However, as the size of the field site to be characterized increases and the demands of resolution increases, the computational burden increases significantly. A computationally efficient algorithm therefore must be developed for speedy analysis of the THT surveys. For basin-scale naturally recurrent tomographic surveys (such as river stage tomography, *Yeh et al.* [2004]), development of such a technology is imperative.

[7] In this study, inspired by the moment generating function approach by *Harvey and Gorelick* [1995], we develop the temporal moment generation equation for impulse pumping tests, similar to the recent work by *Li et al.* [2005]. While *Li et al.* [2005] focus on applying temporal moments to a single impulse pumping test, we apply the temporal moments to transient hydraulic tomography. Specifically, we incorporate the zeroth and first temporal moments of well hydrographs into the SSLE inverse approach [*Yeh and Liu*, 2000] for THT. In addition, we implement a loop iteration scheme [*Zhu and Yeh*, 2005] to avoid the effects of sequential addition of moment information. By directly comparing the estimation using the temporal moments with that using transient heads, we thereafter investigate the temporal moment approach in terms of computational efficiency and accuracy of estimation. Last, limitations of the moment approach are discussed.

2. Methodology

2.1. Derivation of Moment Equations

[8] Groundwater flow induced by pumping in three-dimensional, saturated, heterogeneous geologic media is assumed to be described by the following equation:

$$\nabla \cdot [K(\mathbf{x})\nabla H] + Q(\mathbf{x}_p, t) = S_S(\mathbf{x})\frac{\partial H}{\partial t} \tag{1}$$

subject to boundary conditions:

$$H|_{\Gamma_1} = H_1 \quad \text{and} \quad [K(\mathbf{x})\nabla H]\cdot \mathbf{n}|_{\Gamma_2} = q,$$

and initial condition:

$$H(\mathbf{x})|_{t=0} = H_0(\mathbf{x}) \tag{2}$$

In equation (1), H is the total head (L), $\mathbf{x}$ is the spatial coordinate ($\mathbf{x} = \{x, y, z\}$, (L), and z represents the vertical coordinate and is positive upward), $Q(\mathbf{x}_p, t)$ is the pumping rate per unit volume at location $\mathbf{x}_p$, $K(\mathbf{x})$ is the saturated hydraulic conductivity (L/T), and $S_s(\mathbf{x})$ is the specific storage (L^{-1}). In equation (2), H_1 is the prescribed total head at Dirichlet boundary Γ_1, q is the specific flux (L/T) at Neumann boundary Γ_2, $\mathbf{n}$ is a unit vector normal to the boundary, and $H_0(\mathbf{x})$ represents the initial total head distribution under a steady state condition.

[9] If we define drawdown as $s = H - H_0$, then the drawdown form of the three-dimensional saturated flow equation is given by

$$\nabla \cdot [K(\mathbf{x})\nabla s] + \nabla \cdot [K(\mathbf{x})\nabla H_0] + Q(\mathbf{x}_p, t) = S_s(\mathbf{x})\frac{\partial s}{\partial t} \tag{3}$$

with boundary and initial conditions:

$$s|_{\Gamma_1} = 0, \quad [K(\mathbf{x})\nabla s]\cdot \mathbf{n}|_{\Gamma_2} = q - K\cdot \nabla H_0, \text{ and } s|_{t=0} = 0. \tag{4}$$

In equation (3), $\nabla \cdot [K(\mathbf{x})\nabla H_0]$ represents the divergence of the regional flow prior to pumping tests and is zero as long as it is steady. Applying a moment generating function approach [*Harvey and Gorelick*, 1995] to the drawdown-time data, the nth temporal moments of drawdown at location $\mathbf{x}_i$ are given by

$$M_n(\mathbf{x}_i) = \int_0^\infty t^n s(\mathbf{x}_i, t)dt \tag{5}$$

where $M_n(x_i)$ is the nth temporal moment of drawdown at location $\mathbf{x}_i$. Notice that $Y = M_1/M_0$ is a characteristic time depicting the arrival time of the center of the area under a drawdown-recovery curve. Multiplying equation (3) with t^n and integrating over time from 0 to infinite gives

$$\int_0^\infty t^n \nabla \cdot [K(\mathbf{x})\nabla s]dt + \int_0^\infty t^n \nabla \cdot [K(\mathbf{x})\nabla H_0]dt + \int_0^\infty t^n Q(\mathbf{x}_p, t)dt = \int_0^\infty t^n S_s(\mathbf{x})\frac{\partial s}{\partial t}dt \quad (6)$$

Substituting equation (5) into equation (6), assuming that the regional flow is steady (i.e., the second term on the left-hand side of equation (6) is zero), and that the duration of pumping at location $\mathbf{x}_p$ with a constant rate of Q is τ, and using integration by parts for the right-hand term, we obtain the moment equation:

$$\nabla \cdot [K(\mathbf{x})\nabla M_n] + Q(\mathbf{x}_p)\frac{\tau^{n+1}}{n+1} = S_s(\mathbf{x})st^n\Big|_{t=0}^{t=\infty} - S_s(\mathbf{x})nM_{n-1} \quad (7)$$

Applying the same procedure to equation (4), the boundary conditions for equation (7) become

$$M_n|_{\Gamma_1} = 0 \quad \text{and} \quad K(\mathbf{x})\frac{\partial M_n}{\partial x_i}\cdot \mathbf{n}|_{\Gamma_2} = \int_0^\infty t^n(q - K\nabla H_0)dt \quad (8)$$

Letting $n = 0$ in equation (7) leads to the zeroth moment equation

$$\nabla \cdot [K(\mathbf{x})\nabla M_0] + Q(\mathbf{x}_p)\tau = S_S(\mathbf{x})s\big|_{t=0}^{t=\infty} \quad (9)$$

The zeroth moment represents the area under the drawdown-recovery curve. The solution to equation (9) requires our knowledge of drawdown at every point in the solution domain at both initial and final time. While drawdown at t = 0 is generally zero everywhere, the spatial distribution of the drawdown in a real-world aquifer after pumping starts is difficult to know with a limited number of wells and current technologies. The final drawdown throughout the aquifer however will be zero after pumping is stopped and enough time is allowed for aquifer to recover. If this is the case, then, equation (9) becomes

$$\nabla \cdot [K(\mathbf{x})\nabla M_0] + Q(\mathbf{x}_p)\tau = 0 \quad (10)$$

The associated boundary conditions are

$$M_0|_{\Gamma_1} = 0 \quad \text{and} \quad K(\mathbf{x})\frac{\partial M_0}{\partial x_i}\cdot \mathbf{n}|_{\Gamma_2} = \int_0^\infty (q - K\nabla H_0)dt \quad (11)$$

Now, setting $n = 1$ in equation (7), the governing equation for the first moment is

$$\nabla \cdot [K(\mathbf{x})\nabla M_1] + Q(\mathbf{x}_p)\frac{\tau^2}{2} + S_S(\mathbf{x})M_0 = 0 \quad (12)$$

The associated boundary conditions are

$$M_1|_{\Gamma_1} = 0 \quad \text{and} \quad K(\mathbf{x})\frac{\partial M_1}{\partial x}\cdot \mathbf{n}|_{\Gamma_2} = \int_0^\infty t(q - K\nabla H_0)dt \quad (13)$$

Equations (10), (11), (12), and (13) are essentially the governing equations for the zeroth and first temporal moments of drawdown anywhere in the aquifer induced by a single pumping during a hydraulic tomographic survey. They are identical to those equations developed by *Li et al.* [2005] for an aquifer test that involves one pumping location in an aquifer. By using the moments of the drawdown, a parabolic equation (i.e., equation (1)) has been transformed to two Poisson's equations (equations (10) and (12)). In other words, the governing transient groundwater flow equation is replaced by two steady equations which can be solved directly without using any time march scheme.

2.2. Sequential Inverse Algorithm

[10] Our estimation technique using drawdown moments from hydraulic tomography is based on the sequential successive linear estimator (SSLE) developed by *Yeh et al.* [1996], *Zhang and Yeh* [1997], *Li and Yeh* [1999], *Hughson and Yeh* [2000], *Vargas-Guzman and Yeh* [1999, 2002], *Yeh and Liu* [2000], *Liu and Yeh* [2004], and, in particular, *Zhu and Yeh* [2005]. We first assume that the natural logs of saturated hydraulic conductivity and specific storage are stochastic processes. One advantage of using the natural logarithm is that it avoids negative values of the parameters during the estimation. We then assume $\ln K = \overline{K} + f$ and $\ln S_s = \overline{S} + b$, where ln denotes natural logarithm; $\overline{K}$ and $\overline{S}$ are mean values; f and b denote the perturbations. Similarly, the zeroth moment of drawdown induced by a pumping test during transient hydraulic tomography can be decomposed into two parts: $M_0 = \overline{M}_0 + m_0$, where $\overline{M}_0$ is the mean and m_0 is the perturbation. The characteristic time Y can also be decomposed as $Y = \overline{Y} + y$, where $\overline{Y}$ is the mean and y is the perturbation. Expanding the zeroth moment and characteristic time in a Taylor series about the mean values of parameters, and neglecting second- and higher-order terms, the perturbations at location i can be expressed as:

$$m_{0i} = f_j\frac{\partial M_{0i}}{\partial \ln K_j}\Big|_{\overline{K},\overline{S}} = \mathbf{f}\mathbf{J}_{M_0 \ln K} \quad y_i = f_j\frac{\partial Y_i}{\partial \ln K_j}\Big|_{\overline{K},\overline{S}} + b_j\frac{\partial Y_i}{\partial \ln S_{Sj}}\Big|_{\overline{K},\overline{S}} = \mathbf{f}\mathbf{J}_{Y \ln K} + \mathbf{b}\mathbf{J}_{Y \ln S_S} \quad (14)$$

where a repeated subscript implies summation of its range. In equation (14), f_j and b_j are perturbation of $\ln K$ and $\ln S_S$ at location j and j = 1, ...N, which is the total number of elements in the domain, and they are denoted by matrices $\mathbf{f}$ and $\mathbf{b}$. The sensitivity matrices of M_0 and Y at location i with respect to $\ln K$ and $\ln S_S$ perturbation at location j are given by $\mathbf{J}_{M_0 \ln K} = \frac{\partial M_{0i}}{\partial \ln K_j}$, $\mathbf{J}_{Y \ln K} = \frac{\partial Y_i}{\partial \ln K_j}$ and $\mathbf{J}_{Y \ln S} = \frac{\partial Y_i}{\partial \ln S_j}$. Assuming K and S_s are independent from each other, the covariances of m_0 and y, and the cross covariance between m_0 and f, between y and f, and between y and b can be obtained by a first-order analysis and is expressed as

$$\begin{aligned}
\mathbf{R}_{m_0 m_0}(\mathbf{x}_i, \mathbf{x}_j) &= \mathbf{J}_{M_0 \ln K}\mathbf{R}_{ff}(\mathbf{x}_i, \mathbf{x}_j)\mathbf{J}^T_{M_0 \ln K} \\
\mathbf{R}_{yy}(\mathbf{x}_i, \mathbf{x}_j) &= \mathbf{J}_{Y \ln K}\mathbf{R}_{ff}(\mathbf{x}_i, \mathbf{x}_j)\mathbf{J}^T_{Y \ln K} + \mathbf{J}_{Y \ln S_S}\mathbf{R}_{bb}(\mathbf{x}_i, \mathbf{x}_j)\mathbf{J}^T_{Y \ln S_S} \\
\mathbf{R}_{m_0 f}(\mathbf{x}_i, \mathbf{x}_j) &= \mathbf{J}_{M_0 \ln K}\mathbf{R}_{ff}(\mathbf{x}_i, \mathbf{x}_j) \\
\mathbf{R}_{yb}(\mathbf{x}_i, \mathbf{x}_j) &= \mathbf{J}_{Y \ln S_S}\mathbf{R}_{bb}(\mathbf{x}_i, \mathbf{x}_j) \\
\mathbf{R}_{yf}(\mathbf{x}_i, \mathbf{x}_j) &= \mathbf{J}_{Y \ln K}\mathbf{R}_{ff}(\mathbf{x}_i, \mathbf{x}_j)
\end{aligned} \quad (15)$$

where $\mathbf{R}_{ff}(\mathbf{x}_i, \mathbf{x}_j)$ and $\mathbf{R}_{bb}(\mathbf{x}_i, \mathbf{x}_j)$ are covariance matrices of f and b between location $\mathbf{x}_i$ and $\mathbf{x}_j$, respectively. $\mathbf{R}_{m_0 f}(\mathbf{x}_i, \mathbf{x}_j)$, $\mathbf{R}_{yf}(\mathbf{x}_i, \mathbf{x}_j)$, $\mathbf{R}_{yb}(\mathbf{x}_i, \mathbf{x}_j)$ are cross-covariance matrices between m_0 and f, y and f, and y and b, respectively. $\mathbf{R}_{m_0 m_0}(\mathbf{x}_i, \mathbf{x}_j)$ and $\mathbf{R}_{yy}(\mathbf{x}_i, \mathbf{x}_j)$ are covariance matrices of m_0 and y, respectively. The superscript T represents the transpose of the matrix.

[11] The estimate of f at location $\mathbf{x}_i$, $\hat{f}(\mathbf{x}_i)$, is then derived using a linear multivariate estimator:

$$\hat{f}(\mathbf{x}_i) = \alpha_j f_j^* + \lambda_k m_{0k}^* + \beta_\ell y_\ell^* \quad j = 1, \ldots N_f; \quad k = 1, \ldots N_{m_0}; \quad \ell = 1, \ldots N_y \tag{16}$$

where α_j, λ_k and β_l are weights. N_f, N_{m_0} and N_y are the total number of f, zeroth moment, and characteristic time measurements, respectively. Measurements for hydraulic conductivity, zeroth moment, and characteristic time are denoted by f^*, m_0^*, and y^*, respectively. Similarly, the estimate of b at location $\mathbf{x}_i$, $\hat{b}(\mathbf{x}_i)$, is given by

$$\hat{b}(\mathbf{x}_i) = \varepsilon_n b_n^* + \mu_\ell y_\ell^* \quad n = 1, \ldots N_b; \quad \ell = 1, \ldots N_y \tag{17}$$

where ε_n and μ_k are weights, and N_b is the total number of b^*'s, which are specific storage measurements. All weights are evaluated based on the covariance and cross covariances (equation (15)) [see *Hughson and Yeh*, 2000]. Our inverse algorithm then successively updates parameter estimates and residual covariances and sequentially includes data sets from different pumping tests. The updating and sequentially inclusion procedures are not presented here. Detailed derivations are described by *Hughson and Yeh* [2000] for inversion of unsaturated flow, *Yeh and Liu* [2000] for hydraulic tomography, and *Yeh et al.* [2002] for electrical resistivity tomography.

2.3. Evaluation of Moment Sensitivities

[12] The SSLE approach requires evaluation of the sensitivity matrices. To reduce the computational cost, these sensitivities are evaluated by an adjoint state method [*Sykes et al.*, 1985; *Sun and Yeh*, 1992]. A detailed derivation of the sensitivities is given at Appendix A. The sensitivity of M_0 to ln$K$ is given by

$$\frac{\partial M_0^k}{\partial \ln K_\ell} = \int_\Omega -\frac{\partial \phi_0^*}{\partial \mathbf{x}} K_\ell \frac{\partial M_0}{\partial \mathbf{x}} d\Omega. \tag{18}$$

The sensitivity of M_1 to ln$K$ is given by

$$\frac{\partial M_1^k}{\partial \ln K_\ell} = \int_\Omega \left[-\frac{\partial \phi_0^*}{\partial \mathbf{x}} K_\ell \frac{\partial M_0}{\partial \mathbf{x}} - \frac{\partial \phi_1^*}{\partial \mathbf{x}} K_\ell \frac{\partial M_1}{\partial \mathbf{x}} \right] d\Omega, \tag{19}$$

and the sensitivity of M_1 to lnS_S is given as

$$\frac{\partial M_1^k}{\partial \ln S_{S\ell}} = \int_\Omega \phi_1^* M_0 S_{s_\ell} d\Omega, \tag{20}$$

where ϕ_0^* and ϕ_1^* are arbitrary functions which are defined in Appendix A; the superscript k denotes the observation at location $\mathbf{x}_k$ and the subscript ℓ denotes the location of the parameter in the domain Ω. To evaluate Equations (18), the arbitrary functions ϕ_0^* must be known a priori. ϕ_0^* is obtained by solving the adjoint equation (A16). On the other hand, to calculate the sensitivity of M_1 to ln$K$ or lnS_s (Equations (19) and (20)), the adjoint equations (A9) and (A10) are solved sequentially. That is, we derive ϕ_1^* first and then use it in equation (A10) to obtain ϕ_0^*.

[13] Both moment equation (10) and equation (12) are Poisson's equations, which need to be solved only once, as opposed to the parabolic equation of the governing equation for transient groundwater flow, which must be solved for each time step. As a consequence, significant computational costs can be reduced during evaluation of sensitivity matrices. Consider that the hydrograph at an observation well has been recorded at a 1 s interval for a period of 100 s during an impulse pumping test. Suppose that this hydrograph is used directly to estimate the hydraulic properties and the adjoint state method is employed to evaluate the associated sensitivity matrices. For each drawdown measurement at a given time, an associated adjoint equation must be solved once. The adjoint equation for transient flow is a parabolic equation [see *Zhu and Yeh*, 2005]. For each given time, the solution to the adjoint equation must be obtained by a backward time-marching scheme to derive the sensitivity of drawdown with respect to a parameter. If the computational time step in the evaluation of the sensitivity is assumed to be the same as the sampling interval (1 s), the total number of times that the adjoint matrix equations need to be solved for the 100 measurements will be 5050 (i.e., a sum of the numbers from 1 to 100). Since drawdowns are highly correlated in time, the number of drawdown measurements used in the estimation can be reduced [*Zhu and Yeh*, 2005]. Say, if only three samples at 40, 60, and 80 s from the 100 measurements of the hydrograph are selected for the sensitivity analysis, then the total number of times the system equation for the arbitrary function needs to be solved is reduced to 180.

[14] Now, suppose that we use the moment approach. Instead of using the 3 transient drawdown measurements, only the zeroth and first moments of the hydrograph are needed. Subsequently, one only has to solve the adjoint equation for the zeroth moment equation (A16) once and then the two adjoint equations for first moment equation, equation (A9) and equation (A10). That is, only three system equations have to be solved for the sensitivity analysis. Here, the example considers just one observation well. As the number of observation wells increases, the difference becomes even more significant. The temporal moments approach thus is computationally efficient, compared to the drawdown-time approach.

[15] Notice that the zeroth-moment equation (equation (10)) only depends on the hydraulic conductivity. As a result, the influence of the specific storage is avoided during estimation of the hydraulic conductivity even under transient flow conditions.

3. Numerical Examples

[16] We created a 2-D heterogeneous confined aquifer to compare computational cost between temporal moments and transient heads approaches for the hydraulic tomography analysis. Since temporal moments are integrated forms of a well hydrograph, they may lose some information that reflects effects of heterogeneity at different parts of an

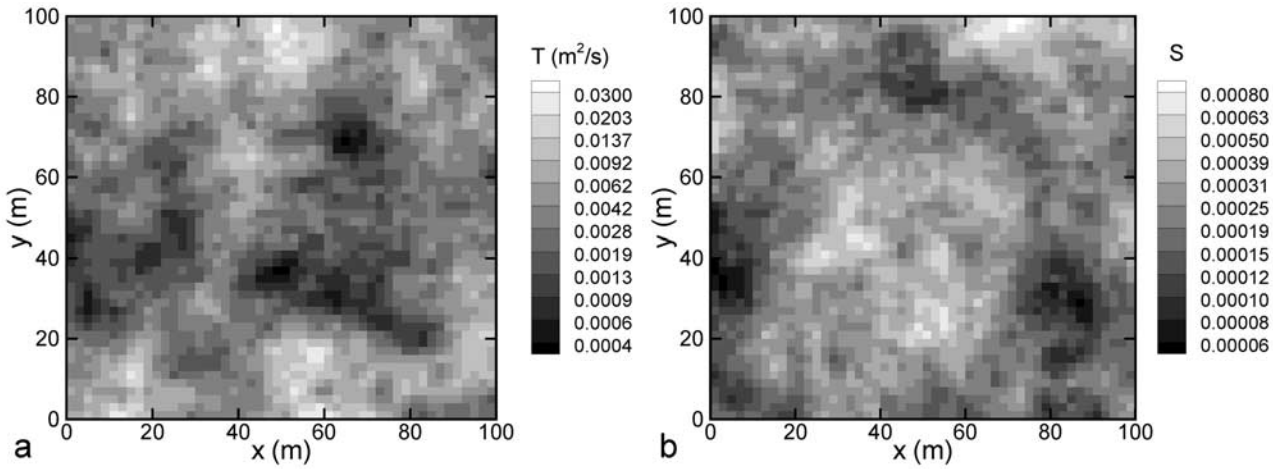

Figure 1. True synthetic fields: (a) transmissivity and (b) storage coefficient.

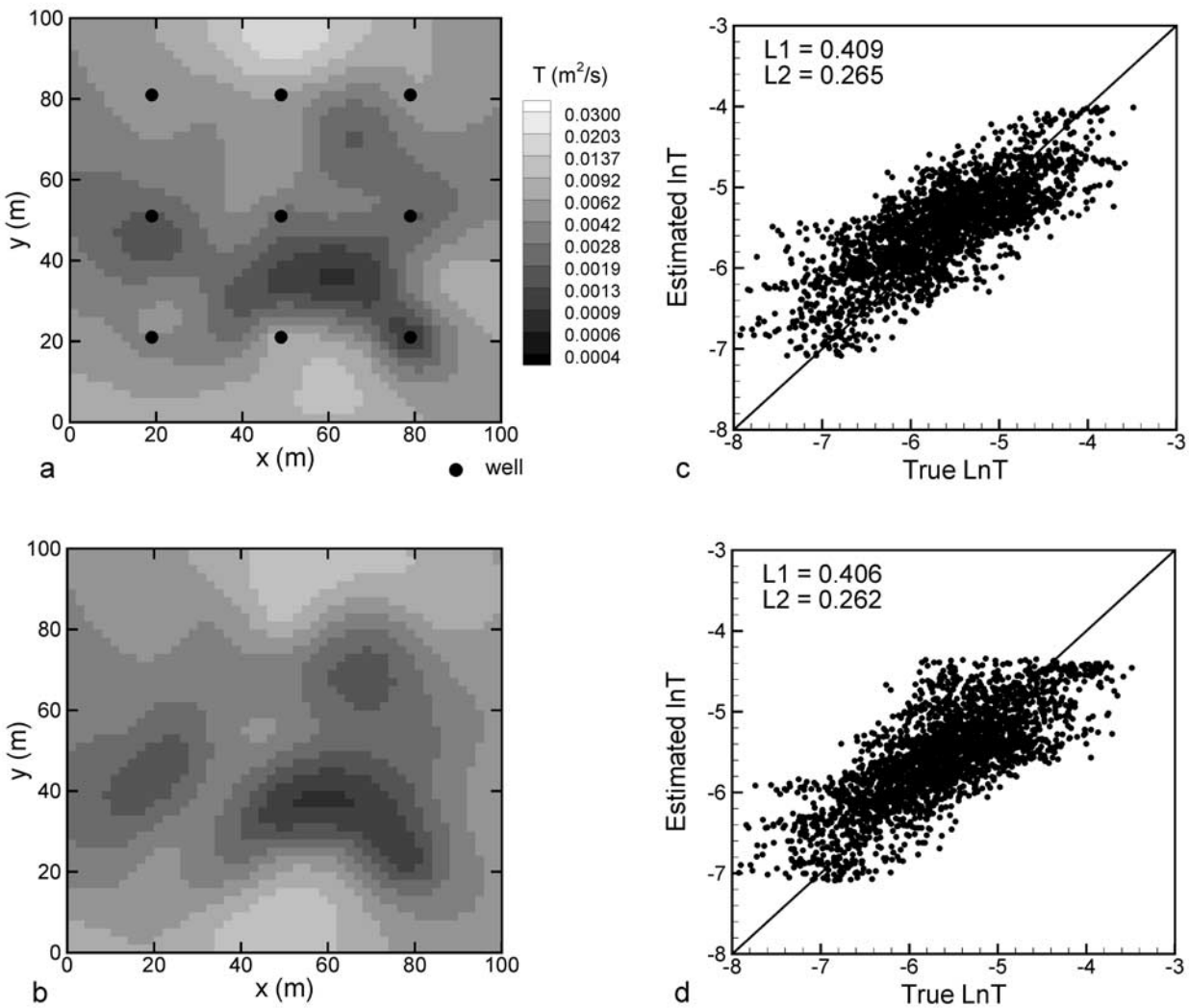

Figure 2. Estimated transmissivity fields using a sparse well field. (a) Using transient heads (case 1), (b) using temporal moments (case 2), (c) the scatterplot of estimated versus true ln$T$ fields of case 1, and (d) the scatterplot of estimated versus true ln$T$ field of case 2.

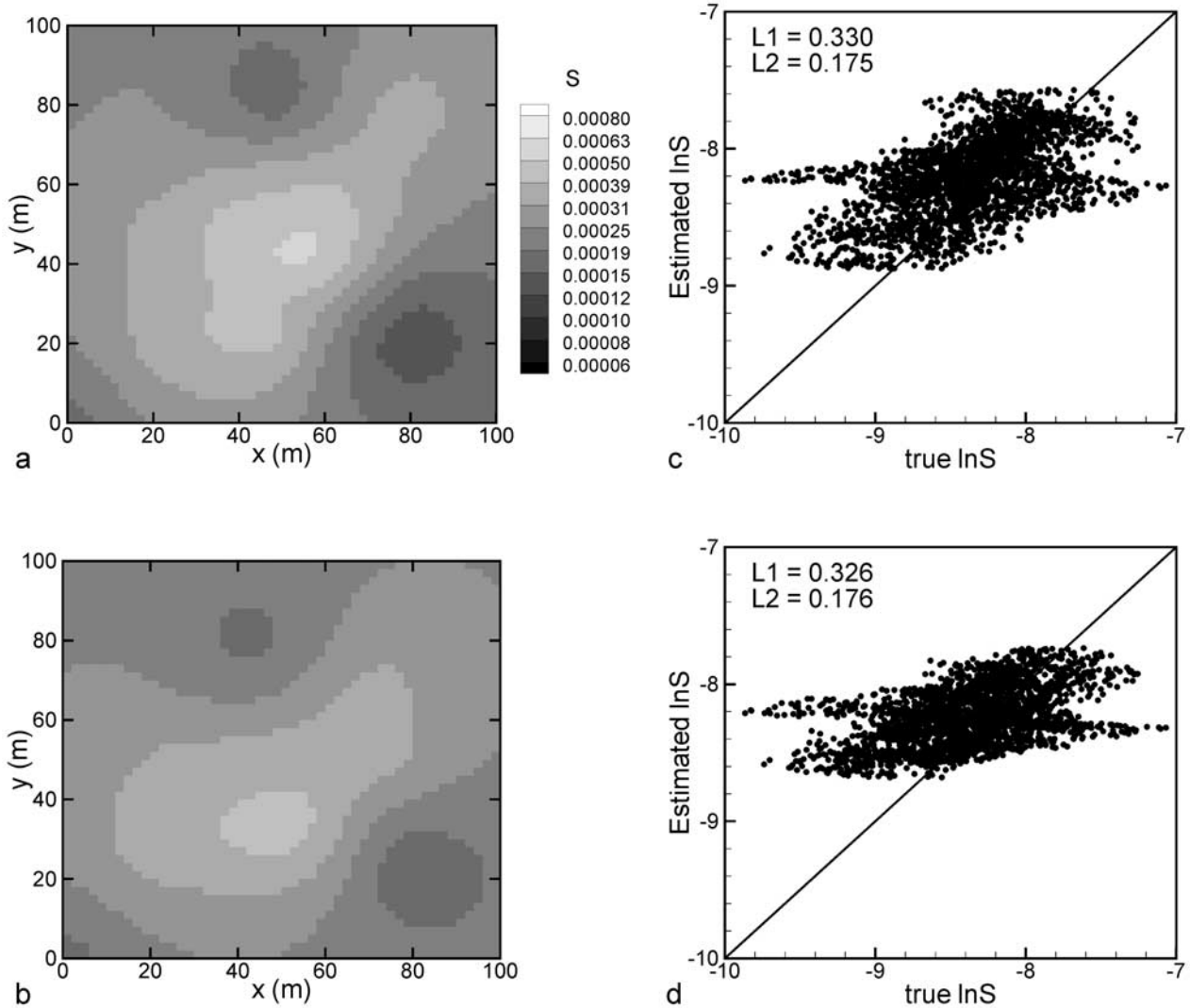

Figure 3. Estimated storage coefficient fields using a sparse well field. (a) Using transient heads (case 1), (b) using temporal moments (case 2), (c) the scatterplot of estimated versus true ln$S$ fields of case 1, and (d) the scatterplot of estimated versus true ln$S$ field of case 2.

aquifer as the cone of depression evolves. This loss of information may be significant, especially since only the first two moments are considered. Therefore we also investigated the impacts of information loss on our estimates of hydraulic properties.

[17] The aquifer considered is 100 m long and 100 m wide and is discretized into 2500 elements with a dimension of 2 m by 2 m. The aquifer has spatially varying transmissivity (T) and storage coefficient (S) fields. Both T and S fields are generated by a spectral random field generator [*Gutjahr*, 1989]. The geometric mean of the T field is 0.0035 m^2/s and the variance of ln$T$ for the field is 0.6. Meanwhile, the geometric mean of the S field and its variance in term of ln$S$ are 0.00023 and 0.2, respectively. The correlation scales for materials in both the x direction and y direction are assumed to be 20 m. Figure 1 plots the generated T and S fields. All boundaries of the aquifer as well as its initial head distribution are assigned to be a constant head of 100 m. Four cases are simulated. Case 1 involves nine wells uniformly distributed on a grid with the distance between two adjacent wells 1.5 times the correlation length of the aquifer properties (see Figure 2 for well locations). This case represented a sparse monitoring network. Nine pumping tests were sequentially simulated at these wells with a pumping rate of 0.1 m^3/s. The pumping time for each pumping test lasted 50 s and then the pumping stopped to allow a full recovery. During each pumping test, head responses were obtained from the nine wells, and we thus have 81 hydrographs after the hydraulic tomography survey. According to *Zhu and Yeh* [2005], a few selected transient heads in a hydrograph are needed to obtain accurate estimates of hydraulic properties during hydraulic tomography. On the basis of their findings we selected the transient heads collected at 10, 30, 50, 70, 100, and 200 s to estimate T and S simultaneously. These sampling times were selected to capture the behaviors of the rising and falling limbs of the hydrograph.

[18] The well field of case 1 was used in case 2 but zeroth moments and characteristic times of the drawdown at the nine wells due to nine sequential pumpings are used to

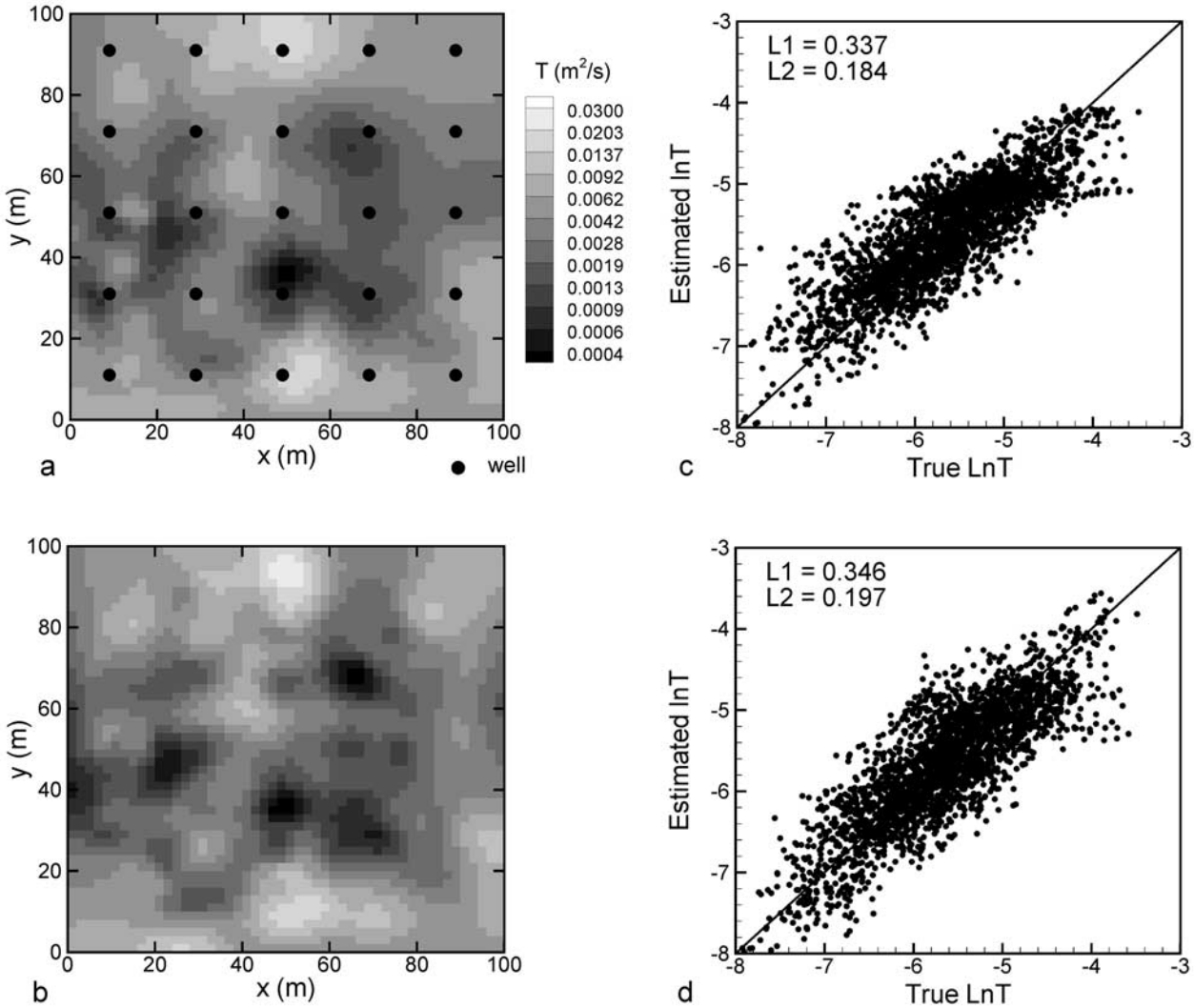

Figure 4. Estimated transmissivity fields using a dense well field. (a) Using transient heads (case 3), (b) using temporal moments (case 4), (c) the scatterplot of estimated versus true ln$T$ fields of case 3, and (d) the scatterplot of estimated versus true ln$T$ field of case 4.

estimate T and S. Since determining the time to fully reach recovery is difficult, calculating moments from the drawdown-recovery curve could introduce some measurement error. Introducing measurement errors could obscure the comparison. Consequently, these moments in case 2 are simulated directly from moment equations (10) and (12) for this case. In practice, estimating moments from observed hydrographs would inevitably involve some errors, but they are difficult to quantify in a simple manner.

[19] An "optimal" monitoring network based on the results by *Yeh and Liu* [2000] is considered in case 3. In this case, 25 observation wells (see Figure 4 for well locations) were added to the aquifer, which are distributed with a distance (20 m) between two adjacent wells (i.e., one correlation length). The pumping wells are the same as the nine used in case 2. As a result, we had 25 well hydrographs for each pumping test and a total of 225 well hydrographs after the nine sequential pumping tests. Similar to case 1, we selected the transient heads collected at 10, 30, 50, 70, 100, and 200 s for estimating T and S. The corresponding moment approach of case 3 is presented as case 4. Instead of using the head data, 225 pairs of the zeroth moments and characteristic times from the 25 wells were simulated for the nine sequential pumping. Then, the moments were used in the estimation. The four numerical cases were executed on a PC-Cluster of 4 processors (Pentium 4, 2.8 GHz, 1G memory each) platform. The simulation times for the four cases were 423.8, 64.4, 766.1, and 179.2 min, respectively. Figure 2 compares the estimated transmissivity fields of case 1 and case 2. Comparison of the estimated storage coefficient fields for these two cases is shown in Figure 3. Estimated transmissivity fields of cases 3 and 4 are shown in Figure 4, and Figure 5 compares estimated storage coefficient fields for these two cases.

4. Results and Discussion

[20] Results of the 2-D synthetic case shows that case 2 (the moment approach) uses only 15.2% of the computation time needed for case 1 (the head approach); likewise, case 4

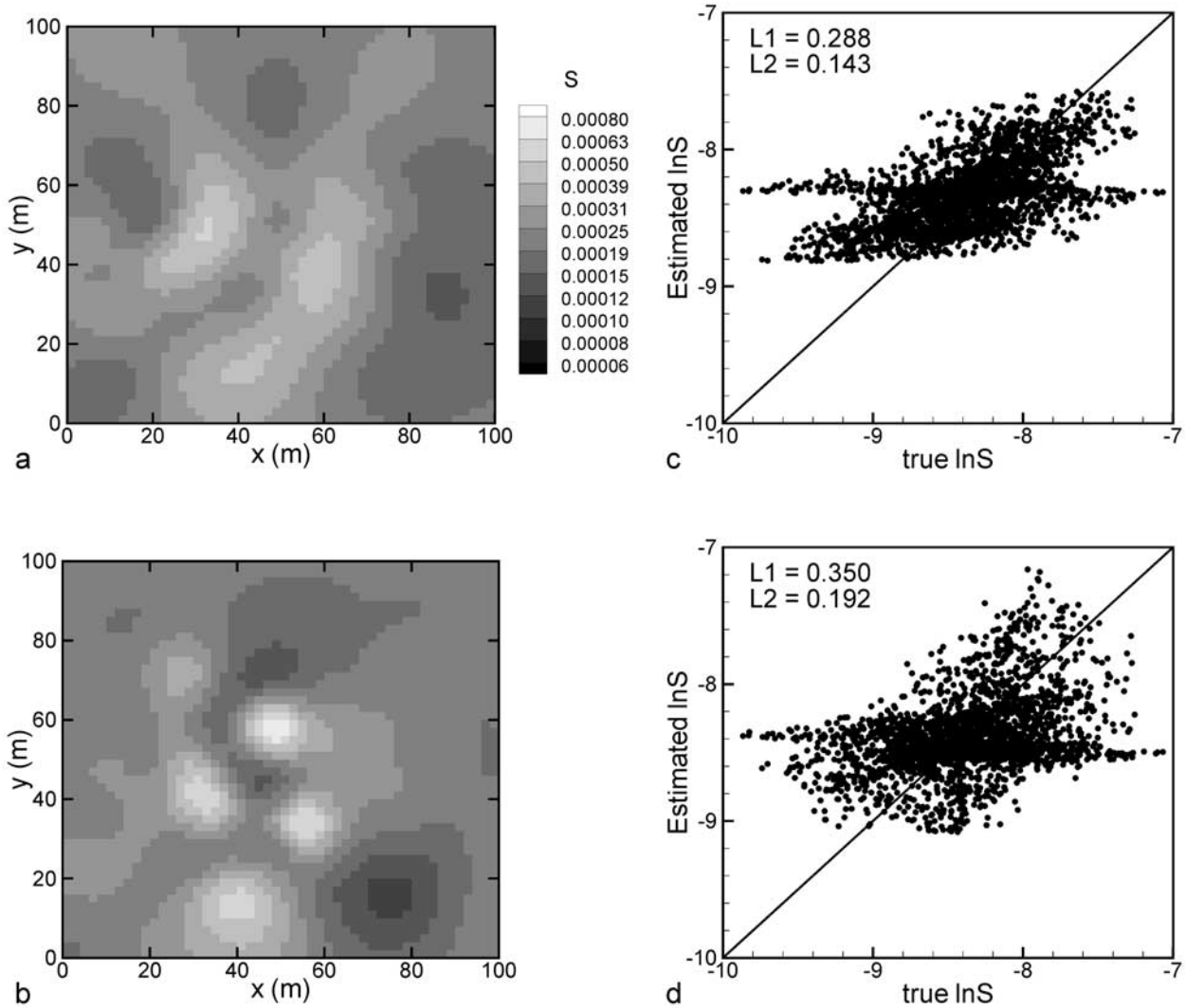

Figure 5. Estimated storage coefficient fields using a sparse well field. (a) Using transient heads (case 3), (b) using temporal moments (case 4), (c) the scatterplot of estimated versus true ln$S$ fields of case 3, and (d) the scatterplot of estimated versus true ln$S$ field of case 4.

(the moment approach) uses only 23.4% of the time needed for case 3. These results substantiate our speculation about the computational efficiency of the temporal moments approach. In order to quantitatively compare the estimation errors, we plot scatterplots of estimates versus true fields for all four cases in Figures 2–5, along with mean absolute error normal L1 and mean square error normal L2, which are defined as

$$L1 = \frac{1}{n}\sum_{i=1}^{n}|\chi_i - \hat{\chi}_i| \quad \text{and} \quad L2 = \frac{1}{n}\sum_{i=1}^{n}(\chi_i - \hat{\chi}_i)^2 \qquad (21)$$

where χ_i and $\hat{\chi}_i$ represent the true and estimates of the log-transformed parameter (either ln$T$ or ln$S$), respectively, i indicates the element number, and n is the total number of elements. According to Figures 2–5, the moment approach based on the first two temporal moments of drawdown can yield similar estimates of transmissivity and storage coefficient fields as those based on transient heads. We also test biasness of our estimations by calculating mean and variance of estimation error, which are defined as

$$\mu = \frac{1}{n}\sum_{i=1}^{n}(\hat{\chi}_i - \chi_i) \quad \text{and} \quad \sigma^2 = \frac{1}{n}\sum_{i=1}^{n}((\hat{\chi}_i - \chi_i) - \mu)^2 \qquad (22)$$

where μ and σ^2 are mean and variance of difference between true and estimated parameter (either ln$T$ or ln$S$). The mean and variance of estimation errors are list in Table 1. They show that SSLE yields unbiased estimations in all cases. As expected, a dense monitoring network can produce much better results than a sparse network. It is clear however that

Table 1. Mean and Variance of Estimation Errors

	Case 1		Case 2		Case 3		Case 4	
	ln$T$	ln$S$	ln$T$	ln$S$	ln$T$	ln$S$	ln$T$	ln$S$
Mean	0.1496	0.0756	0.1642	0.1360	0.0264	−0.0211	0.0499	−0.0124
Variance	0.2435	0.2563	0.1485	0.1575	0.1835	0.1962	0.1410	0.1918

the results based on the temporal moments are not identical to those based on the transient heads.

[21] The use of the dense and sparse monitoring networks in the above synthetic cases is aimed at investigating the impact of information loss in the moments approach on the inverse results. Transient well hydrographs intuitively bear signatures of the heterogeneity encountered by the drawdown as the cone of depression evolves. These signatures, however, are likely weak because the head recorded at an observation well is highly correlated with different heterogeneities within the cone of depression [*Wu et al.*, 2005]. Because of the integrative nature of the zeroth and first moments of a hydrograph, these moments likely lose these signatures. We therefore anticipate that the interpretation of a hydraulic tomography survey using the temporal moments will yield fewer details about the heterogeneity. Plots of estimated T and S fields and their associated scatterplots in Figures 2 and 3, and statistics of the estimation errors in Table 1 seem to support our hypothesis. The variances of the estimation errors are consistently smaller for the estimated fields based on drawdown than those based on temporal moments. On the other hand, in cases 3 and 4 where the monitoring networks are dense, the differences between the estimated fields based on the two approaches are small. In other words, the information loss in the temporal moments is largely compensated for by the dense spatial information.

[22] The storage coefficient estimates from both transient head and temporal moment approaches in both cases are clearly less satisfactory than transmissivity estimates. This may be attributed to the fact that high cross correlation between head and storage coefficient is limited to a narrow region in between pumping and observation wells; the cross correlation between head and transmissivity on the other hand is strong over the entire cone of depression at late time [*Wu et al.*, 2005].

[23] Notice that in all cases examined here, the temporal moments at observation wells were directly obtained from moment equations (10) and (12). Such a direct evaluation has omitted possible errors in estimating the moments from well hydrographs. Effects of errors in the moments on the estimates of transmissivity and storage coefficient have been studied by *Li et al.* [2005] during a single aquifer test. According to their study, the effects are not significant. Obviously, rigorous analysis of impacts of errors in moments on hydraulic tomography is necessary but it is beyond the scope of this paper.

5. Conclusions

[24] The temporal moment approach significantly reduces computational cost for interpreting transient hydraulic tomography. The cost reduction is attributed to the fact that the governing equations for the temporal moments are Poisson's equations. As a consequence, the forward modeling required for improving new estimates of transmissivity and storage coefficients does not have to solve the parabolic equation that governs groundwater flow. The parabolic equation in general has to be solved by a time marching scheme, implying that a system of equations must be evaluated at each time step. Avoiding solving the system of equations for each time step thus reduces computational efforts. Furthermore, the adjoint equations for evaluating sensitivity matrices of temporal moments are also Poisson's equations. In our SSLE and some other inverse models, the adjoint equations are solved for each measurement during each iteration of the estimation process. Again, without evaluating time-dependent adjoint equations, computational burdens during evaluation of sensitivity are reduced. This reduction is particularly significant when the number of temporal and spatial observations is large.

[25] The temporal moment approach for interpreting hydraulic tomography is unequivocally more efficient than the approach using transient head data directly. The differences in results of the moment and head approaches are small if a dense network is used. Furthermore, for the situations where only hydraulic conductivity is of interest, the zeroth temporal moment of transient well hydrograph can be used to estimate transmissivity without involving the estimation of the storage coefficient. This unique characteristic of the temporal moment approach makes the approach highly attractive for practical applications.

Appendix A: Derivation of Moment Sensitivities Using the Adjoint State Method

[26] Differentiating the zeroth-moment equation,

$$\nabla \cdot [K(\mathbf{x})\nabla M_0] + Q(\mathbf{x}_p)\tau = 0 \tag{A1}$$

with respect to a parameter χ (where χ represent $\ln K$ or $\ln S$ at any location in the spatial domain Ω) give

$$\frac{\partial}{\partial \mathbf{x}}\left(\frac{\partial K}{\partial \chi}\frac{\partial M_0}{\partial \mathbf{x}}\right) + \frac{\partial}{\partial \mathbf{x}}\left(K\frac{\partial \phi_0}{\partial \mathbf{x}}\right) = 0 \tag{A2}$$

where $\phi_0 = \partial M_0/\partial \chi$ is called state sensitivity. Multiplying the resultant equation by an arbitrary function, ϕ_0^*, and integrating the equation over the entire spatial domain, Ω, gives

$$\int_\Omega \left[\phi_0^*\frac{\partial}{\partial \mathbf{x}}\left(\frac{\partial K}{\partial \chi}\frac{\partial M_0}{\partial \mathbf{x}}\right) + \phi_0^*\frac{\partial}{\partial \mathbf{x}}\left(K\frac{\partial \phi_0}{\partial \mathbf{x}}\right)\right] d\Omega = 0. \tag{A3}$$

Applying Green's theorems to both terms of the left hand side of equation (A3) yields the following equation,

$$\int_\Omega \left[-\frac{\partial \phi_0^*}{\partial \mathbf{x}}\frac{\partial K}{\partial \chi}\frac{\partial M_0}{\partial \mathbf{x}} + \phi_0\frac{\partial}{\partial \mathbf{x}}\left(K\frac{\partial \phi_0^*}{\partial \mathbf{x}}\right)\right] d\Omega + \int_\Gamma \left[\phi_0^*\frac{\partial K}{\partial \chi}\frac{\partial M_0}{\partial \mathbf{x}} + \phi_0^* K\frac{\partial \phi_0}{\partial \mathbf{x}} - \phi_0 K\frac{\partial \phi_0^*}{\partial \mathbf{x}}\right]\cdot \mathbf{n}\, d\Gamma = 0 \tag{A4}$$

Applying a similar procedure to the first-moment equation,

$$\nabla \cdot [K(\mathbf{x})\nabla M_1] + Q(\mathbf{x}_p)\frac{\tau^2}{2} + S_S(\mathbf{x})M_0 = 0, \tag{A5}$$

we obtain

$$\int_\Omega \left[-\frac{\partial \phi_1^*}{\partial \mathbf{x}}\frac{\partial K}{\partial \chi}\frac{\partial M_1}{\partial \mathbf{x}} + \phi_1\frac{\partial}{\partial \mathbf{x}}\left(K\frac{\partial \phi_1^*}{\partial \mathbf{x}}\right) + \phi_1^*\frac{\partial S_s}{\partial \chi}M_0 + \phi_1^*\phi_0 S_s\right] d\Omega + \int_\Gamma \left[\phi_1^*\frac{\partial K}{\partial \chi}\frac{\partial M_1}{\partial \mathbf{x}} + \phi_1^* K\frac{\partial \phi_1}{\partial \mathbf{x}} - \phi_1 K\frac{\partial \phi_1^*}{\partial \mathbf{x}}\right]\cdot \mathbf{n}\, d\Gamma = 0 \tag{A6}$$

where ϕ_1^* is another arbitrary function and $\phi_1 = \partial M_1/\partial\chi$ is another state sensitivity. The marginal sensitivity of a performance measure P is given as

$$\frac{dP}{d\chi} = \int_\Omega \left(\frac{\partial G}{\partial \chi} + \frac{\partial G}{\partial M_0}\phi_0 + \frac{\partial G}{\partial M_1}\phi_1\right) d\Omega \tag{A7}$$

where G is the state function. The first term in the right side of equation (A7) represents direct dependence of the performance measure on the parameter whereas the second and third terms provide indirect dependence of the performance measure on the parameter through moments. Next, we add equation (A4) and equation (A6) into equation (A7), yielding

$$\begin{aligned}\frac{dP}{d\chi} = \int_\Omega \Bigg[&\frac{\partial G}{\partial \chi} + \frac{\partial G}{\partial M_0}\phi_0 + \phi_0 \frac{\partial}{\partial \mathbf{x}}\left(K\frac{\partial \phi_0^*}{\partial \mathbf{x}}\right) + \phi_1^*\phi_0 S_s + \frac{\partial G}{\partial M_1}\phi_1 \\ &+ \phi_1 \frac{\partial}{\partial \mathbf{x}}\left(K\frac{\partial \phi_1^*}{\partial \mathbf{x}}\right) - \frac{\partial \phi_0^*}{\partial \mathbf{x}}\frac{\partial K}{\partial \chi}\frac{\partial M_0}{\partial \mathbf{x}} - \frac{\partial \phi_1^*}{\partial \mathbf{x}}\frac{\partial K}{\partial \chi}\frac{\partial M_1}{\partial \mathbf{x}} \\ &+ \phi_1^*\frac{\partial S_s}{\partial \chi}M_0\Bigg] d\Omega + \int_\Gamma \left[\phi_0^*\frac{\partial K}{\partial \chi}\frac{\partial M_0}{\partial \mathbf{x}} + \phi_0^* K\frac{\partial \phi_0}{\partial \mathbf{x}} - \phi_0 K\frac{\partial \phi_0^*}{\partial \mathbf{x}}\right] \\ &\cdot \mathbf{n}\, d\Gamma + \int_\Gamma \left[\phi_1^*\frac{\partial K}{\partial \chi}\frac{\partial M_1}{\partial \mathbf{x}} + \phi_1^* K\frac{\partial \phi_1}{\partial \mathbf{x}} - \phi_1 K\frac{\partial \phi_1^*}{\partial \mathbf{x}}\right]\cdot \mathbf{n}\, d\Gamma.\end{aligned} \tag{A8}$$

If we let the two arbitrary functions ϕ^*_0 and ϕ^*_1 satisfy the following two adjoint equations:

$$\frac{\partial}{\partial \mathbf{x}}\left(K\frac{\partial \phi_1^*}{\partial \mathbf{x}}\right) + \frac{\partial G}{\partial M_1} = 0 \tag{A9}$$

$$\frac{\partial}{\partial \mathbf{x}}\left(K\frac{\partial \phi_0^*}{\partial \mathbf{x}}\right) + \phi_1^* S_s + \frac{\partial G}{\partial M_0} = 0 \tag{A10}$$

and the boundary conditions

$$\phi_n^* = 0 \quad \text{at} \quad \Gamma_1 \tag{A11}$$

$$(K\nabla\phi_n^*)\cdot \mathbf{n} = 0 \quad \text{at} \quad \Gamma_2 \quad (n = 0, 1), \tag{A12}$$

The terms associating with state sensitivities ϕ_0 and ϕ_1 as well as boundary terms in equation (8) disappear. Equation (A8) is reduced to

$$\frac{dP}{d\chi} = \int_\Omega \left[\frac{\partial G}{\partial \chi} - \frac{\partial \phi_0^*}{\partial \mathbf{x}}\frac{\partial K}{\partial \chi}\frac{\partial M_0}{\partial \mathbf{x}} - \frac{\partial \phi_1^*}{\partial \mathbf{x}}\frac{\partial K}{\partial \chi}\frac{\partial M_1}{\partial \mathbf{x}} + \phi_1^*\frac{\partial S_s}{\partial \chi}M_0\right] d\Omega \tag{A13}$$

If an observation of the moments is made at location, $\mathbf{x}_k$, the state function becomes $G = M_n\delta(\mathbf{x} - \mathbf{x}_k)$ in which $n = 0$, and 1, denoting the zero and the first moment, respectively. Now, let $G = M_1\delta(\mathbf{x} - \mathbf{x}_k)$ be the first moment at location $\mathbf{x}_k$, the direct dependence term, $\partial G/\partial\chi$, becomes zero. If K and S_s are uncorrelated, then the term, $\partial S_s/\partial \ln K$ in equation (A13) is zero. As a result, we have the sensitivity of M_1^k with respect to $\ln K_\ell$:

$$\frac{\partial M_1^k}{\partial \ln K_\ell} = \int_\Omega \left[-\frac{\partial \phi_0^*}{\partial \mathbf{x}}K_\ell\frac{\partial M_0}{\partial \mathbf{x}} - \frac{\partial \phi_1^*}{\partial \mathbf{x}}K_\ell\frac{\partial M_1}{\partial \mathbf{x}}\right] d\Omega \tag{A14}$$

where the superscript k denotes the observation at location $\mathbf{x}_k$ and the subscript ℓ denotes the location of the parameter in the domain. Similarly, the sensitivity of M_1 to $\ln S_S$ is given as

$$\frac{\partial M_1^k}{\partial \ln S_{S\ell}} = \int_\Omega \phi_1^* M_0 S_{s_\ell} d\Omega. \tag{A15}$$

Next, let $G = M_0\delta(\mathbf{x} - \mathbf{x}_k)$ be the zeroth moment at location $\mathbf{x}_k$, then term, $\partial G/\partial M_1$, in equation (A9) is zero. As a result, the solution ϕ_1^* of adjoint equation (A9) is zero everywhere. The adjoint equation (A10) therefore is reduced to

$$\frac{\partial}{\partial \mathbf{x}}\left(K\frac{\partial \phi_0^*}{\partial \mathbf{x}}\right) + \frac{\partial G}{\partial M_0} = 0, \tag{A16}$$

and equation (A13) becomes

$$\frac{dP}{d\chi} = \int_\Omega \left[\frac{\partial G}{\partial \chi} - \frac{\partial \phi_0^*}{\partial \mathbf{x}}\frac{\partial K}{\partial \chi}\frac{\partial M_0}{\partial \mathbf{x}}\right] d\Omega. \tag{A17}$$

The sensitivity of M_0 to $\ln K$ is then given as

$$\frac{\partial M_0^k}{\partial \ln K_\ell} = \int_\Omega -\frac{\partial \phi_0^*}{\partial \mathbf{x}}K_\ell\frac{\partial M_0}{\partial \mathbf{x}} d\Omega \tag{A18}$$

[27] **Acknowledgments.** The work reported was supported by NSF grant EAR-0229717, a SERDP grant subcontracted through University of Iowa, NSF IIS-0431079, and NSF EAR-0450388. We are grateful for useful and constructive comments from Associate Editor and three anonymous reviewers.

References

Beckie, R., and C. F. Harvey (2002), What does a slug test measure: An investigation of instrument response and the effects of heterogeneity, *Water Resour. Res.*, *38*(12), 1290, doi:10.1029/2001WR001072.

Bohling, G. C., X. Zhan, J. J. Butler Jr., and L. Zheng (2002), Steady shape analysis of tomographic pumping tests for characterization of aquifer heterogeneities, *Water Resour. Res.*, *38*(12), 1324, doi:10.1029/2001WR001176.

Brauchler, R., R. Liedl, and P. Dietrich (2003), A travel time based hydraulic tomographic approach, *Water Resour. Res.*, *39*(12), 1370, doi:10.1029/2003WR002262.

Gottlieb, J., and P. Dietrich (1995), Identification of the permeability distribution in soil by hydraulic tomography, *Inverse Probl.*, *11*, 353–360.

Gutjahr, A. (1989), Fast Fourier transforms for random field generation, *N. M. Tech. Proj. Rep. Contract 4-R58-2690 R*, N. M. Inst. of Min. and Technol., Socorro.

Harvey, C. F., and S. M. Gorelick (1995), Temporal moment-generating equations: Modeling transport and mass transfer in heterogeneous aquifers, *Water Resour. Res.*, *31*(8), 1895–1912.

Hughson, D. L., and T.-C. J. Yeh (2000), An inverse model for three-dimensional flow in variably saturated porous media, *Water Resour. Res.*, *36*(4), 829–839.

Li, B., and T.-C. J. Yeh (1999), Cokriging estimation of the conductivity field under variably saturated flow conditions, *Water Resour. Res.*, *35*(12), 3663–3674.

Li, W., W. Nowak, and O. A. Cirpka (2005), Geostatistical inverse modeling of transient pumping tests using temporal moments of drawdown, *Water Resour. Res.*, *41*, W08403, doi:10.1029/2004WR003874.

Liu, S., and T.-C. J. Yeh (2004), An integrative approach for monitoring water movement in the vadose zone, *Vadose Zone J.*, *3*, 681–692.

Liu, S., T.-C. J. Yeh, and R. Gardiner (2002), Effectiveness of hydraulic tomography: Sandbox experiments, *Water Resour. Res.*, *38*(4), 1034, doi:10.1029/2001WR000338.

Oliver, D. S. (1993), The influence of nonuniform transmissivity and storativity on drawdown, *Water Resour. Res.*, *29*(1), 169–178.

Sun, N.-Z., and W. W.-G. Yeh (1992), A stochastic inverse solution for transient groundwater flow: Parameter identification and reliability analysis, *Water Resour. Res.*, *28*(12), 3269–3280.

Sykes, J. F., J. L. Wilson, and R. W. Andrews (1985), Sensitivity analysis for steady state groundwater flow using adjoint operators, *Water Resour. Res.*, *21*(3), 359–371.

Vargas-Guzman, A. J., and T.-C. J. Yeh (1999), Sequential kriging and cokriging: Two powerful geostatistical approaches, *Stochastic Environ. Res. Risk Assess.*, *13*, 416–435.

Vargas-Guzman, A. J., and T.-C. J. Yeh (2002), The successive linear estimator: A revisit, *Adv. Water Resour.*, *25*, 773–781.

Vasco, D. W., H. Keers, and K. Karasaki (2000), Estimation of reservoir properties using transient pressure data: An asymptotic approach, *Water Resour. Res.*, *36*(12), 3447–3465.

Vesselinov, V. V., S. P. Neuman, and W. A. Illman (2001), Three-dimensional numerical inversion of pneumatic cross-hole tests in unsaturated fractured tuff: 2. Equivalent parameters, high-resolution stochastic imaging and scale effects, *Water Resour. Res.*, *37*(12), 3019–3042.

Wu, C.-M., T.-C. J. Yeh, J. Zhu, T. H. Lee, N.-S. Hsu, C.-H. Chen, and A. F. Sancho (2005), Traditional analysis of aquifer tests: Comparing apples to oranges?, *Water Resour. Res.*, *41*, W09402, doi:10.1029/2004WR003717.

Yeh, T.-C. J. (1992), Stochastic modeling of groundwater flow and solute transport in aquifers, *J. Hydrol. Processes*, *6*, 369–395.

Yeh, T.-C. J. (1998), Scale issues of heterogeneity in vadose-zone hydrology, in *Scale Dependence and Scale Invariance in Hydrology*, edited by G. Sposito, Cambridge Univ. Press, New York.

Yeh, T.-C. J., and S. Liu (2000), Hydraulic tomography: Development of a new aquifer test method, *Water Resour. Res.*, *36*(8), 2095–2105.

Yeh, T.-C. J., M. Jin, and S. Hanna (1996), An iterative stochastic inverse approach: Conditional effective transmissivity and head fields, *Water Resour. Res.*, *32*(1), 85–92.

Yeh, T.-C. J., K. Hsu, C. Lee, J. Wen, and C. Ting (2004), On the possibility of using river stage tomography to characterize the aquifer properties of the Choshuishi Alluvial Fan, Taiwan, *Eos Trans. AGU*, *85*(47), Fall Meet. Suppl., Abstract H11D-0329.

Zhang, J., and T.-C. J. Yeh (1997), An iterative geostatistical inverse method for steady flow in the vadose zone, *Water Resour. Res.*, *33*(1), 63–71.

Zhu, J., and T.-C. J. Yeh (2005), Characterization of aquifer heterogeneity using transient hydraulic tomography, *Water Resour. Res.*, *41*, W07028, doi:10.1029/2004WR003790.

T.-C. J. Yeh and J. Zhu, Department of Hydrology and Water Resources, University of Arizona, 1133 East North Campus Drive, Tucson, AZ 85721, USA. (ybiem@mac.hwr.arizona.edu)